



## Development of an equipment for real-time continuous monitoring of alpha and beta radioactivity in river water

A. Tarancón<sup>a,c,d,\*</sup>, O. Novella<sup>b,1</sup>, M. Pujadas<sup>b</sup>, M. Batlle<sup>b</sup>, J. Cros<sup>b</sup>, J.F. García<sup>a,d,\*\*</sup>

<sup>a</sup> Department of Analytical Chemistry of the University of Barcelona, Spain

<sup>b</sup> Adasa Sistemas S.A.U, Spain

<sup>c</sup> Serra-Hunter Program, Spain

<sup>d</sup> Water Research Institute of the University of Barcelona, Spain

### ABSTRACT

Different regulations require the monitoring of radioactivity in the environment (e.g., 2013/51/Euratom, Real Decreto 314/2016) to protect the environment and the population from abnormal radioactivity presence caused by natural reasons or discharges or accidents in nuclear installations. Nowadays, the monitoring of  $\alpha$ - and  $\beta$ -emitting radionuclides is performed discontinuously in laboratories due to the difficulties in applying classical techniques to continuous measurements. This limits the number of samples that can be measured per day, produces high costs per analysis, and introduces a significant delay between the moment of contamination and when it is detected. Plastic scintillation microspheres (PSm) represent a new possibility for continuous measurements because water samples can flow through a bed of PSm connected to a pair of photomultipliers (PMTs), allowing continuous monitoring of the activity. This idea is the basis of the Waterrad detector, which can monitor radioactivity at environmental levels in river water. This paper describes the optimization of a detection cell containing PSm, a detection chamber as well as active and passive shielding. In its final set-up, the Waterrad detector presents a background signal of 0.23 (1) cps and detection efficiencies of  $1.86(7)\cdot 10^{-5}$  cps·L·Bq<sup>-1</sup> for <sup>3</sup>H,  $7.4(8)\cdot 10^{-3}$  cps·L·Bq<sup>-1</sup> for <sup>90</sup>Sr/<sup>90</sup>Y and  $5.5(5)\cdot 10^{-3}$  cps·L·Bq<sup>-1</sup> for <sup>241</sup>Am. The detection limits in the optimum window for a counting time of 5 h were 490 Bq/L for <sup>3</sup>H, 2.3 Bq/L for <sup>90</sup>Sr/<sup>90</sup>Y and 3.0 Bq/L for <sup>241</sup>Am. These values indicate that Waterrad can be used as an alarm detector for monitoring radioactivity in water at activity levels similar to those of environmental samples, making it suitable for water or waste surveillance involving a high frequency of measurements.

### 1. Introduction

Different regulations require the monitoring of radioactivity in rivers to protect the population and the environment from controlled radioactive discharges or illegal and accidental releases from nuclear installations or terrorist activities. Following the recommendation of the WHO (WHO, 2018), the Council Directive 2013/51/Euratom of 22 October 2013 (the Council of the European Union, 2013) states the guide levels that should be established by the law of each member state of the European Union. In the case of Spain, the Real Decreto 314/2016 (de España, 2016) states that the monitoring is the responsibility of the supplier and that the parametric values are 0.1 mSv for the indicative dose, 100 Bq/L for tritium and 500 Bq/L for radon. Assessment of the indicative dose is made first through screening strategies based on measuring gross alpha activity (0.1 Bq/L) and gross beta activity (1 Bq/L). If these screening parameters exceed the limits, the analysis of specific alpha- and beta-emitting radionuclides is required.

The analytical methodology used depends on the methods available, which determine the accuracy and limits of detection that can be achieved and the periodicity of the analysis. The analysis of gamma emitters can be performed using continuous monitoring equipment that takes advantage of the high power of penetration of the gamma rays and the possibility to have adequate distance between the sample and the detector (Cantaluppi et al., 2021). However, the emitters that mainly contribute to the radioactive doses ingested by humans are the alpha and beta emitters. The detection of these types of emitters is not so easy, since the range of these particles is so short that the sample must be in contact with the detector to produce a measurable signal (L' Annunziata, 2020). Common methods used to measure alpha-emitting radionuclides, such as alpha spectrometry and proportional counting, follow this approach, but cannot be applied in continuous measurements due to the complexity of the measurement process (Sobiech-Matura et al., 2017). (Jobb á gy et al., 2010). Regarding liquid scintillation, which is a valid method to analyze both alpha and beta emitters, there are some

\* Corresponding author. Department of Analytical Chemistry of the University of Barcelona, Spain.

\*\* Corresponding author. Department of Analytical Chemistry of the University of Barcelona, Spain.

E-mail addresses: [alex.tarancón@ub.edu](mailto:alex.tarancón@ub.edu) (A. Tarancón), [jfgarcia@ub.edu](mailto:jfgarcia@ub.edu) (J.F. García).

<sup>1</sup> Independent professional (current position).

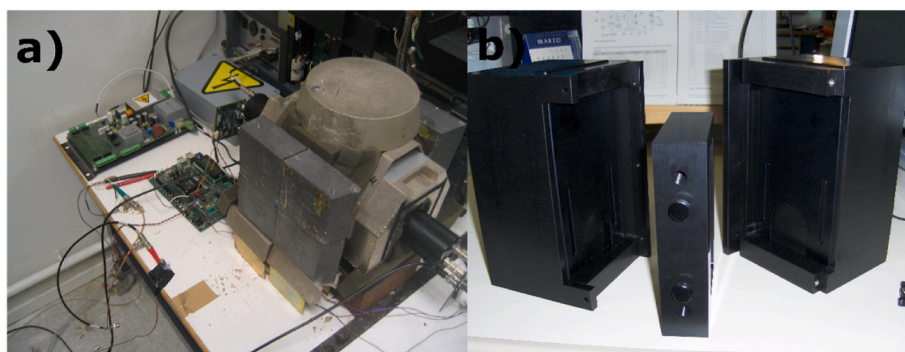


Fig. 1. (a) Radilevel, (b) detection chamber.

commercial detectors that are used for continuous measurements in biology and medicine (Hou and Roos, 2008). (Hou, 2018). However, they cannot be used in environmental monitoring due to some drawbacks, which include difficulties in obtaining a stable mixture of the organic scintillator and the water sample, the use of large amounts of the scintillation cocktail, and the generation of significant quantities of mixed waste (radioactive and harmful) (Hofstetter and Wilson, 1992). (Sigg et al., 1994).

Plastic scintillators have also been used in the analysis of radioactivity, taking advantage of the simplicity of a system based on a solid scintillator that is in contact with the water sample in a counting chamber. As the scintillator is solid, there is no continuous consumption of reagents and no wastes are generated, which are critical for equipment located in remote areas and operating in an automated way without maintenance. However, the different types of equipment described to date are not capable of achieving the low limits of detection required for environmental monitoring. This is because the active volume is small due to the large distance between most parts of the sample and the scintillator (usually in the form of fibers or sheets), leading to detection efficiencies that are too low for environmental monitoring (Köll, 2015; Lee et al., 2019; Lv et al., 2018; Azevedo et al., 2020).

Recently, plastic scintillation microspheres (PSm) have been proposed as an alternative to liquid scintillators in the measurement of alpha and beta particles since their scintillation capacities are comparable (Tarancón et al., 2017; Lluch et al., 2016; Bliznyuk et al., 2015). For continuous measurements, the PSm can be placed in a cell and the water sample can flow through the microspheres, which means that there is no scintillator consumption or the generation of mixed wastes (Tarancón et al., 2005; Hughes and DeVol, 2006). In addition, as the microspheres are around 50–100  $\mu\text{m}$  in size, the distance an alpha or beta particle has to travel in the water medium before it reaches the microsphere is low enough to give a high probability of detection. This makes the active volume very high, therefore producing detection efficiencies that are similar or slightly lower than those obtained with liquid scintillators for alpha emitters and medium- or high-energy beta emitters. For low-energy beta emitters, such as  $^3\text{H}$ , the probability is lower, but the beta particles can still be detected with acceptable efficiencies (Santiago et al., 2016).

In this article, we present the development and optimization of a continuous monitoring detector of radioactivity based on PSm. The analysis was centered on the development of a measuring cell, a field-programmable gate array (FPGA)-based electronics, active and passive shielding to reduce background, and hydraulics. Finally, the detection efficiency and the limit of detection were established and the equipment was tested in the laboratory for the analysis of water samples from the Ebro River.

## 2. Experiments

### 2.1. Reagents, solutions and materials

Two types of PSm were used. First, studies were performed with PSm (UPS-89) supplied by Detec-Rad (Ottawa, Canada). The PSm were separated by sieving and the fraction used in this study corresponded to that retained between the sieves with a pore diameter of 250  $\mu\text{m}$  and 350  $\mu\text{m}$  pore diameter. Measurements with the Waterrad detector were performed with the PSm synthesized at the Section of Analytical Chemistry of the University of Barcelona, following the evaporation/extraction method. These PSm were composed of polystyrene, 2,5-diphenyloxazole (PPO), 1,4-bis(5-phenyloxazol-2-yl)benzene (POPOP) and 2,6-diisopropyl-naphthalene (DIN). The proportions of PPO, POPOP and DIN in the microspheres, with regards to polystyrene, were 0.2%, 0.05% and 20%, respectively. The PSm obtained presented a median diameter of 60  $\mu\text{m}$ .

An active guard was built from two 10\*10\*30  $\text{cm}^3$  blocks made of PS (UPS-89) supplied by Detec-Rad (Ottawa, Canada).

When radioactive samples were measured by conventional procedures, they were prepared in 20-mL polyethylene vials (PerkinElmer, USA).

Three radioactive stock solutions were used: a  $^3\text{H}$  solution ( $^3\text{H}_2\text{O}$ ) at a concentration of 3.94 (14) kBq/g prepared from a standard of 69.8 (24) kBq/g (Eckert-Ziegler, Berlin, Germany) in deionized water; a  $^{90}\text{Sr}/^{90}\text{Y}$  active stock solution ( $\text{Sr}^{2+}$  and  $\text{Y}^{3+}$ ) of 37.2 (3) Bq/g prepared from a standard of 4.07 (3) kBq/g (Amersham International) in 0.1 HCl as a carrier solution; and a  $^{241}\text{Am}$  solution ( $\text{Am}^{3+}$ ) of 186 (2) Bq/g prepared from a standard of 55.4 (6) kBq/g (Amersham International) in a solution of 0.5 M HCl and deionized water.

White paint number 11 (Acrylicos Vallejo, Spain) was used as a reflective coating on the active guard PS blocks and the optical connector. Black Acrylic Brillante (Bruger, Spain) was used to blind the active guard PS blocks. A protective colorless acrylic varnish (ALP-Pinturas, Spain) was used to protect them.

Water samples from the Ebro River between García and Flix (41°09'56.2"N 0°36'41.7"E) were used to validate the Waterrad detector.

### 2.2. Apparatus

Measurements were performed in four apparatuses: two commercial ones used as reference to provide comparative data (Wallac 1414 and Wallac 1220 Quantulus) and two apparatuses developed in this study (Radilevel, for the initial design process, and Waterrad, to complete the optimization and for the continuous measurements).

The commercial 1414 liquid scintillation detector (EGG & Wallac) has logarithmic amplification and a multichannel analyzer of 1024 channels. It was modified so that a continuous cell could be placed in the counting chamber with holes for the cell tubes. A specific software was

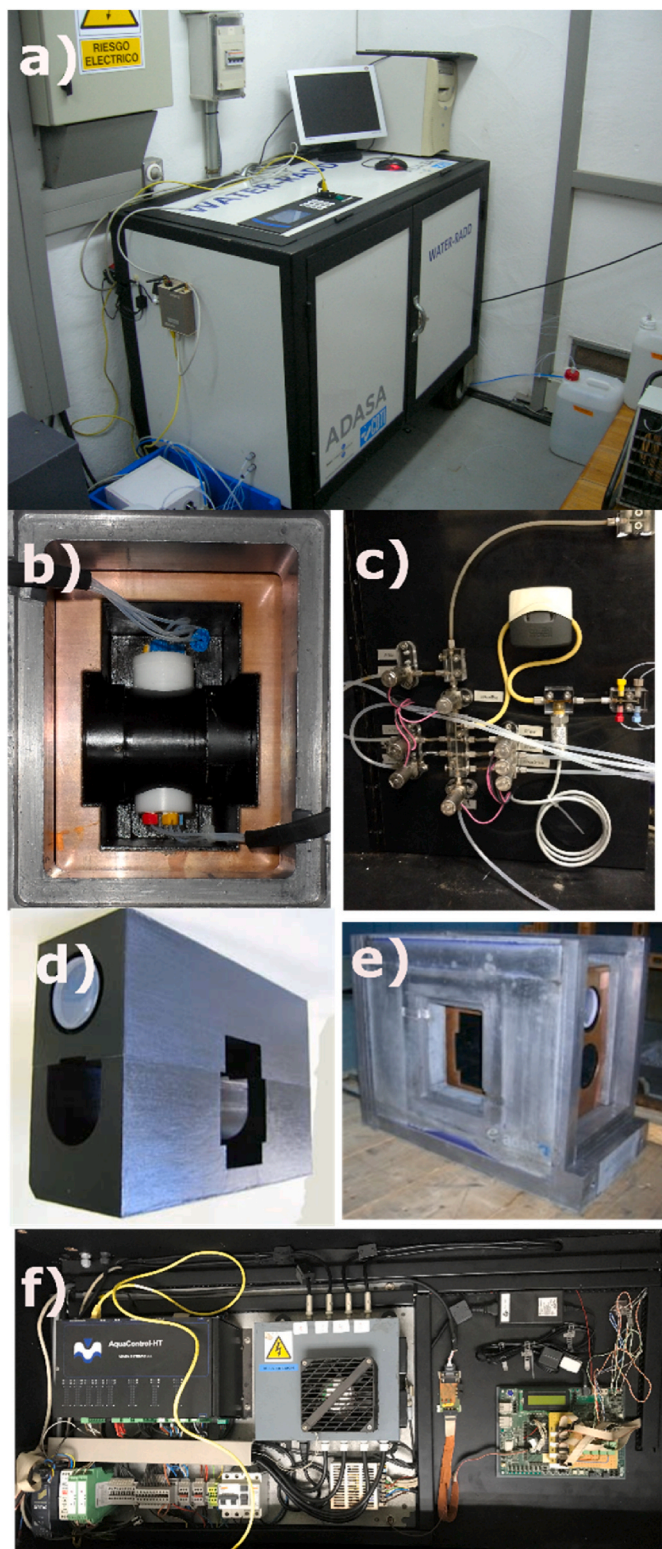


**Figure 2.** (a) Waterrad, (b) detection chamber, (c) hydraulics, (d) passive shielding, (e), active shielding and (f) electronics.

used to control the 1414 detector and manage the files generated.

### 2.2.1. Radilevel

Radilevel, the first prototype of a continuous monitoring detector (Fig. 1a), was composed of the following elements:

- **Detection chamber (Fig. 1b):** this was built in black POM to prevent the entrance of light. The chamber was composed of three blocks: two containing the photomultipliers (PMTs) and the door of the chamber where the cell was placed and through which the tubes entered and exited from the cell. This modular structure permitted the use of cells of different sizes.
- **Shielding:** the shielding of the detector was made using the lead blocks of the 1414 commercial detector since the chamber has similar dimensions to that of the 1414 detector. Moreover, several blocks of lead were placed at the bottom and at the lateral sides of the chamber to reduce cosmic radiation.
- **Electronics:** two R331-05SEL PMTs from Hamamatsu (Hamamatsu City, Japan) were used. Each PMT was connected to a board that filtered the signals, amplified them and generated a square signal when the pulse height is higher than the voltage threshold. Square pulses were sent to a ProASIC 3 A3P250 (Microsemi, Chandler, USA) FPGA of 4 MHz, where pulses were time compared and counted in case of a coincidence. Signals from the PMT boards and the FPGA were also sent to a TDS S024B oscilloscope (Tektronix, Braverton, USA) and to a computer with two MCA cards. The oscilloscope was used to control and register the pulse shape (original and quadratic), whereas the MCA cards counted the coincident pulses and stored the pulse height. The PMTs were fed with an HV source.

Measurements in the Radilevel detector were performed using a voltage threshold of 15 mV and a coincidence time of 20 ns.

### 2.2.2. Waterrad

The Waterrad detector (Fig. 2a) is capable of continuous, autonomous and remote measurements. The elements of the detector were as follows:

- The detection chamber was a cylindrical tube made of POM that connected the two sample PMTs facing one another. The cylinder had two round openings to allow the introduction and extraction of the detection cell inside. The internal part was painted with white reflective paint to improve the transmission of the photons emitted from the cell to the PMTs.
- **Shielding:**
  - o Passive shielding was made of lead blocks of different thicknesses. The dimensions were:  $42*22*10\text{ cm}^3$  for the top block,  $42*22*75\text{ cm}^3$  for the bottom block,  $37*27*5\text{ cm}^3$  for the front and back blocks, and  $27*22*5\text{ cm}^3$  for the lateral blocks. Each lateral block contained two holes that were 6 cm in diameter to allow the entrance of the PMTs. The passive shielding surrounded the active shielding and the detection cell. The front block had a  $12*15*5\text{ cm}^3$  door made of lead to allow the cell to be changed and a hole to allow the entrance and exit of the tubing.
  - o Active shielding involved two blocks of  $30*10*10\text{ cm}^3$  linked with optical grease. Both blocks were painted with white reflective paint to force the internal reflection of the photons produced, as well as with black paint to prevent light entrance and varnish to protect them. The bottom block was mechanized to permit the inside location of the detection cell and two PMTs. The PS blocks were placed in a copper box, which was then placed in the lead shielding.
- **Electronics:**
  - o PMT and PMT boards: Four R331-05SEL PMTs from Hamamatsu were used. Each PMT was connected to a board that filtered the signals, amplified them and generated a square pulse from each signal above a threshold. The original pulse is kept for further analysis (i.e. pulse height)
  - o FPGA board. The signals from the PMT and PMT board were sent to a ProASIC 3 A3P250 FPGA. The FPGA counted the signals, determined coincidences between the PMT signals, determined the pulse amplitude and established the dead time. The FPGA also

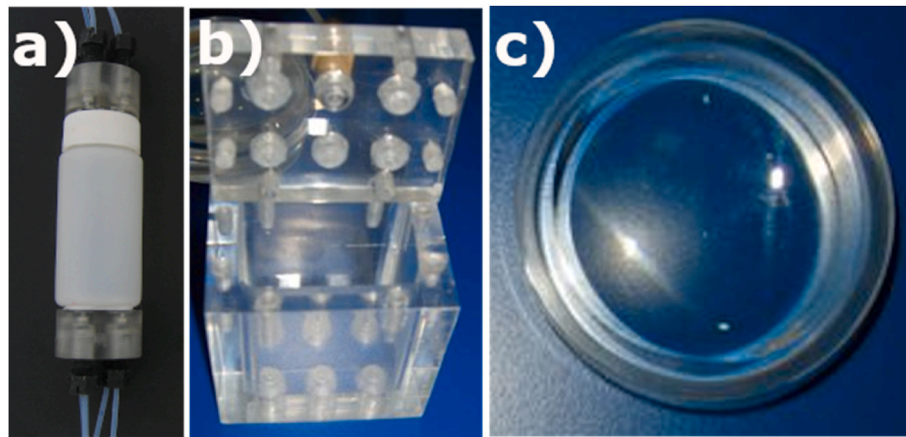


Fig. 3. (a) MOD cell, (b) continuous monitoring cell made of a plastic scintillator (PS) material and a lid also made of PS, and (c) lens made of PS.

generated the voltage signals used as thresholds in the PMT boards.

- o aquaControl module. This module controlled the HV supply and was programmed to control the hydraulics and the configurable parameters of the FPGA (dead time, coincidence time and voltage threshold). The aquaControl module received, every 5 min, all the data stored in the FPGA (counts in each PMT, coincident counts, live time, and the spectrum from each sample PMT) and stored them in its internal memory. The module can be configured through a display and keyboard on the same equipment or remotely using a computer. In remotely the data obtained can be downloaded in a Microsoft Access database.
- Hydraulics: The equipment contained a hydraulic circuit made of a peristaltic pump and valves that were managed with the aquaControl module. The solutions stored were distilled water (for background measurements), as well as the  $^3\text{H}$ ,  $^{90}\text{Sr}/^{90}\text{Y}$  and  $^{241}\text{Am}$  standards (for calibration) and two cleaning solutions (water and 1 M HCl). The hydraulic system had one entrance for the water sample and one exit for the waste.

### 2.2.3. Measurements

Radioactive samples were measured using PE vials or a cell. In both cases, the vials and cells were filled with PSm as the scintillating reagent.

Measurements in PE vials were performed by filling a 20-mL PE vial with 8 mL of solution and 16 g of PSm. The solutions measured were: distilled water, the  $^3\text{H}$  standard, the  $^{90}\text{Sr}/^{90}\text{Y}$  standard and the  $^{241}\text{Am}$  standard. The standard samples had an activity of 800 Bq for  $^3\text{H}$ , and 3.6 Bq for  $^{90}\text{Sr}/^{90}\text{Y}$  and  $^{241}\text{Am}$ . The samples were homogenized using ultrasound for 2 min and centrifugation at 83 Hz for 10 min.

Cell measurements in the 1414 commercial detector and Radilevel were performed to evaluate the different prototypes of the cell. The cells were filled by pumping a volume of 20 mL, which was higher than the volume of the cell. Once the solution was loaded, the flow was stopped and the sample was measured for 60 min. In the second type of measurements, a pulse of active solution of 1 mL was pumped through the cell and the counting rate was measured continuously every 5 s.

Measurements in the Waterrad detector were also performed with the cells. In this case, the solutions were pumped for 10 min since this amount of time was previously established to be enough to ensure cell filling. The flow was then stopped and the sample was measured for 60 min in 5-min periods.

The solutions analyzed were: distilled water,  $^3\text{H}$  standard (19500 Bq/L), the  $^{90}\text{Sr}/^{90}\text{Y}$  standard (58.6 Bq/L) and the  $^{241}\text{Am}$  standard (196.4 Bq/L).

### 2.2.4. Data treatment

Detection efficiencies were calculated as the ratio between the net

count rate and the activity added to the vial or pumped through the cell. Detection efficiency spectrum was obtained by dividing the net count rate spectrum by the total activity (and multiplying by 100 to obtain it in percentage). For continuous measurements, activity is expressed in Bq/L and the detection efficiency in  $\text{cps}\cdot\text{Bq}^{-1}\cdot\text{L}$  or in  $\%\cdot\text{mL}$  since the volume of the cell was not precisely known. For the vial measurements, activity is expressed in Bq and the detection efficiency in percentages.

The detection limit ( $L_D$ ) and critical level ( $L_C$ ) were calculated using the following equations (Currie, 1968):

$$L_C = \frac{2.33 \cdot \sqrt{\frac{\text{Bkg}}{t}}}{e}$$

$$L_D = \frac{\frac{2.71}{t} + 4.65 \cdot \sqrt{\frac{\text{Bkg}}{t}}}{e}$$

where Bkg (in cps) corresponds to the background signal,  $t$  (in s) to the counting time and  $e$  (in  $\text{cps}\cdot\text{L}\cdot\text{Bq}^{-1}$ ) to the detection efficiency. Values of  $L_D$  and  $L_C$  were calculated for the whole spectrum and the optimum windows of  $^3\text{H}$ ,  $^{90}\text{Sr}/^{90}\text{Y}$  and  $^{241}\text{Am}$ .

## 3. Results and Discussion

The development of the continuous monitoring detector was centered on two aspects:

- Optimization of the size, shape and materials of the detection cell.
- Study of the passive and active shielding and other structural components of the equipment.

The tests performed to evaluate the validity of the approaches for the different areas were often undertaken in parallel. This was the case for the detection cell and the electronics. For the structural components and hydraulics, the following were assessed:

- Radilevel: an equipment with basic electronics and hydraulics, with shielding based on lead bricks.
- Waterrad: complete version with all the hydraulics, electronic components as well as active and passive shielding.

The Discussion is centered on the development and optimization of the detection cell and the evaluation of the shielding components. The electronics used for pulse detection, signal treatment and pulse and time counting are described roughly in the Experimental Section, while their performance and characteristics are described in the Discussion. Finally, once the final prototype was obtained, the quality parameters of the equipment were established and a river water sample was measured to

**Table 1**

Detection efficiency for  $^3\text{H}$ ,  $^{90}\text{Sr}/^{90}\text{Y}$  and  $^{241}\text{Am}$  of the MOD cell in a 1414 detector.

Cell	$V_{\text{sample}} = 1 \text{ mL}$		$V_{\text{sample}} > V_{\text{cell}}$	
		Detection efficiency (in %)		Detection efficiency (in %)
$^3\text{H}$	MOD cell	0.24 (2)		1.8 (1)
	20-mL PE Vial	0.31 (1)		2.5 (1)
$^{90}\text{Sr}/^{90}\text{Y}$	MOD cell	169 (3)		1423 (43)
	20-mL PE Vial	177 (1)		1419 (7)
$^{241}\text{Am}$	MOD cell	49 (3)		474 (17)
	20-mL PE Vial	57 (1)		456 (8)

test the performance of the detector.

### 3.1. Cell design and characterization

First cell evaluated was designed on the basis of the previous experience on the measurement of beta and alpha emitting radionuclides with plastic scintillation microspheres (Santiago et al., 2013; Tarancón et al., 2007; Tarancón and Kossert, 2011). This experience indicates that a 20 mL vial cell would be suitable for  $^3\text{H}$  and  $^{241}\text{Am}$  detection, taking into consideration the optical and particle quenching associated to measurement with PSm in this kind of geometry, and sample volume associated. In these conditions it seems possible to achieve acceptable limits of detection for the purpose of the detector.

Three cell designs were evaluated. The first cell developed was a 20-mL PE scintillation vial modified to allow the continuous passage of water through the PSm it contained (Fig. 3a) (hereafter referred to as MOD). This cell contained 16.3 (3) g of PSm and had a sample capacity of 8.5 (5) mL.

The MOD cell filled with PSm was used for the continuous measurement of  $^3\text{H}$ ,  $^{90}\text{Sr}/^{90}\text{Y}$  and  $^{241}\text{Am}$  standard samples in a modified Wallac 1414 detector. Two different scenarios were evaluated. First, the injection of 1 mL of the sample and, second, the injection of a sample volume that was higher than the cell volume to ensure that the cell was completely filled with the sample. In both cases, when the sample was in the cell, the flow was stopped and the measurement started. Therefore, two values were obtained for the detection efficiency (Table 1). The detection efficiency values obtained with 1 mL of the sample were useful in evaluating the scintillation properties of the cell, whereas the detection efficiency values obtained with the higher sample volume permitted the evaluation of the whole cell, including the effects associated with the radionuclide distribution. The values were compared to the detection efficiencies obtained with the  $^3\text{H}$ ,  $^{90}\text{Sr}/^{90}\text{Y}$  and  $^{241}\text{Am}$  standards in the same detector, but using a 20-mL polyethylene vial filled with 16 g of PSm and 8 mL of the standard solution.

The detection efficiencies were higher for the PE vial than for the MOD cell. This difference was greater for  $^3\text{H}$  than for  $^{241}\text{Am}$ , whereas for  $^{90}\text{Sr}/^{90}\text{Y}$ , the differences were small. This correlation of the detection efficiency with the energy as well as with the path of the radioactive particle can be explained by an increase in the space between the microspheres when the measurement was being performed in the modified cell. In the conventional vial, the solution filled the spaces between the microspheres and there was some air in the vial. However, in the MOD cell, the solution and the PSm filled the cell completely, probably decreasing the degree of packing of the microspheres (amount of PSm with regards to the volume of the sample) and increasing the distance between the microspheres. On the contrary, since the volume of sample that filled the continuous monitoring cells was higher, the detection efficiency when the cell was filled with the sample was similar for  $^{241}\text{Am}$  and  $^{90}\text{Sr}/^{90}\text{Y}$ . For  $^3\text{H}$ , the increase in sample volume could not compensate for the decrease in packing and the values remained lower.

**Table 2**

Detection efficiency for  $^3\text{H}$ ,  $^{90}\text{Sr}/^{90}\text{Y}$  and  $^{241}\text{Am}$  of the different cells in the Radilevel detector. Detection efficiencies are given for when the sample volume was 1 mL and higher than the cell volume.

		MOD	CPv1	CP_POM	CP_POM_L	MET
Volume		8.5	9.6	10.2	10.2	11.0
Background (cps)		1.48 (5)	7.99 (8)	7.29 (7)	5.90 (2)	3.62 (6)
$^3\text{H}$	$V = 1 \text{ mL}$	0.134 (17)	0.26 (1)	0.26 (1)	0.197 (6)	0.189 (5)
	$V > V_{\text{cell}}$	0.86 (8)	2.23 (8)	2.22 (8)	1.67 (9)	1.78 (6)
$^{90}\text{Sr}/^{90}\text{Y}$	$V = 1 \text{ mL}$	170 (1)	174 (4)	178 (6)	177 (4)	173 (3)
	$V > V_{\text{cell}}$	1420 (40)	1800 (50)	1730 (30)	1710 (50)	1610 (30)
$^{241}\text{Am}$	$V = 1 \text{ mL}$	45 (3)	57 (3)	55 (3)	47 (3)	51 (2)
	$V > V_{\text{cell}}$	440 (30)	736 (20)	746 (57)	630 (28)	623 (26)

Despite this decrease, the continuous monitoring cell configuration provided similar values to those of a conventional vial, validating the use of this cell for continuous measurements.

The MOD cell was then assessed in the Radilevel detector, which was the first prototype of the continuous monitoring detector. The results (first column in Table 2) showed a decrease in the detection efficiency for  $^3\text{H}$  (when the sample volume was 1 mL and also when the sample volume was higher than the cell volume) with regards to that obtained in the Wallac 1414 detector. The values for  $^{241}\text{Am}$  and  $^{90}\text{Sr}/^{90}\text{Y}$  were similar for the two detectors. This can be explained by the fact that the chamber of the Radilevel detector did not have a reflective coating; therefore, weak scintillating signals, such as those generated from  $^3\text{H}$  disintegrations, were not detected.

To evaluate the effects of different geometries and materials, a new cell, CPv1, was developed (Fig. 3b). CPv1 was a rectangular prism made of plastic scintillator (PS). The inner width was the same as that of a 20-mL polyethylene vial, whereas the two faces that were connected to the PMTs had an outer length that fit the diameter of the PMTs. The walls of the PS cell had a length of 6 mm, which were enough to insert the screws that were used to close the cell with a lid made also of PS. The bottom of the cell and the lid contained six holes to connect the sample tubing. With this configuration, the total volume of the cell was 28.2 mL.

To enhance photon detection, the faces of the cell that were not connected to the PMTs were painted with reflective paint. Moreover, two lenses made of PS were used to connect the PS cell to the PMT. Optical grease was used to ensure optical coupling.

The results obtained with the CPv1 cell and the PS lenses (second column in Table 2) showed a significant increase in the background signals. This could have been due to the addition of more scintillating material (the PS cell and the lenses) to the measuring chamber, since cosmic rays can interact with the PS of the walls of the cell and with the PS lenses, generating more background signals. As can be seen in Fig. 4a, the increase in the count rate took place across the whole spectrum, but was more significant at high energies, indicating that the origin of the signal was the high-energy cosmic radiation.

The improvement in light transmission translated into an increase in the detection efficiency, especially for  $^3\text{H}$ , but also for  $^{241}\text{Am}$ , producing values that were closer to those obtained in the Wallac 1414 commercial detector with 20-mL polyethylene vials. This was also evidenced in the detection efficiency spectrum for  $^{90}\text{Sr}/^{90}\text{Y}$ , which shifted to high channel numbers as the number of photons detected per disintegration increased. Furthermore, the increase in the cell volume, due to a better use of the active area of the PMT, increased the total efficiency.

In terms of the detection limit, since the increase in the total detection efficiency may also be accompanied by an increase in the

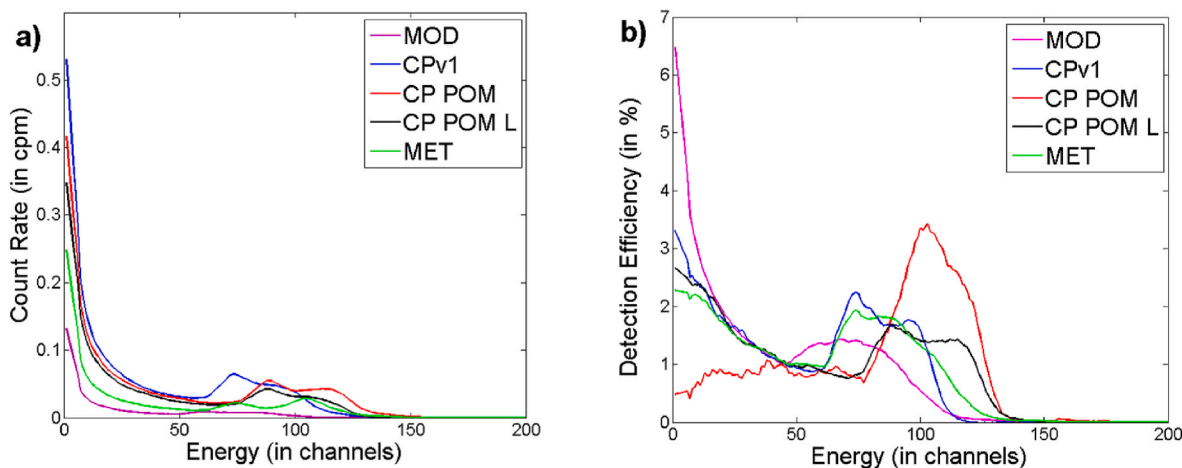


Fig. 4. (a) Background and (b)  $^{90}\text{Sr}/^{90}\text{Y}$  detection efficiency spectra obtained using different cells.

background, the following modifications were made to the detection chamber and the PS cell:

- Substitution of the PS lid of the cell of plastic scintillator by with a lid made of white polyoxymethylene (POM) (CP\_POM)
- Removal of the PS lenses (CP\_POM\_L)
- Use of methacrylate instead of PS to build the cell (MET)

In all the cases, the cells were filled with PSm. The use of the POM lid led to a reduction of the background to 7.3 cps. The detection efficiency for all the isotopes measured was similar to that obtained with the cell made completely of PS (Table 2). When comparing the spectra obtained for  $^{90}\text{Sr}/^{90}\text{Y}$ , it can be seen that the spectrum was located at higher channels. This can be attributed to a better coupling of the cell with the lenses and the lenses with the PMT, consequently improving light transmission. The substitution of a PS lid with a POM lid is therefore recommended.

The removal of the PS lenses also reduced the background to 5.9 cps, but in this case, the detection efficiency also decreased for  $^3\text{H}$  and  $^{241}\text{Am}$ . Moreover, the spectrum for  $^{90}\text{Sr}/^{90}\text{Y}$  was slightly shifted to low energies when compared to that obtained with the cell with lenses and a POM lid. This means that photons were lost in the transmission from the cell to the PMT. Therefore, more optical signals, probably those that were less intense, generated from the  $^3\text{H}$  and  $^{241}\text{Am}$  disintegrations were not detected.

Finally, the substitution of the PS with PMMA in the whole cell produced a relevant reduction of the background (3.62 cps), but the detection efficiency also slightly decreased and the spectrum moved significantly to low channel numbers. It can be concluded that PMMA is not the adequate polymer for scintillation and, consequently, the electrons generated by the cosmic rays or emitted by the radionuclide generate fewer photons than in the PS cell. The background signals registered were mainly due to the PSm in the cell and the PS of the lenses. This is because methacrylate is not transparent at the wavelength of emission of the PSm. Thus, as a consequence of the absorption of photons, the detection efficiency decreased and the spectrum moved to lower energies.

Considering the different cell tested, the one that gave the best results in terms of background was the polyethylene cell. In terms of detection efficiency, the PS cell (with a lid of PS or POM) offered the best results.

The last variable of the cell evaluated was the active volume of the cell, since previous experience with plastic scintillation microspheres indicates that light attenuation (i.e. optical quenching) depends on the size of the PSm and the cell. Then, the smallest the PSm and the highest the cell size are, the lower probability of the photons to escape from

Table 3

Inner volume, mass of PSm, sample volume, background count rate and the detection efficiencies for  $^3\text{H}$ ,  $^{90}\text{Sr}/^{90}\text{Y}$  and  $^{241}\text{Am}$  obtained in continuous measurements with the small-, medium- and large-sized cells.

	Small size	Medium size	Large size
Total inner volume ( $\text{cm}^3$ )	7.1	28.2	77.6
Mass of PSm (g)	4.4 (2)	17.4 (5)	47 (2)
Sample volume (mL)	2.4 (1)	10.0 (3)	29 (2)
Background count rate (cps)	6.6 (4)	7.6 (3)	13.2 (4)
$^3\text{H}$			
V = 1 mL (in %)	0.4 (1)	0.25 (1)	0.030 (7)
Detection efficiency			
V > $V_{\text{cell}}$ (in %·mL)	0.8 (3)	2.23 (4)	0.5 (2)
$^{90}\text{Sr}/^{90}\text{Y}$			
V = 1 mL (in %)	180 (2)	174 (5)	152 (11)
Detection efficiency			
V > $V_{\text{cell}}$ (in %·mL)	418 (55)	1848 (146)	4067 (1215)
$^{241}\text{Am}$			
V = 1 mL (in %)	60.8 (7)	57 (2)	31 (4)
Detection efficiency			
V > $V_{\text{cell}}$ (in %·mL)	137 (11)	676 (110)	797 (192)

these heterogeneous media.

Three PS cells with a POM lid and a width of 6 mm, 24 mm and 64 mm (i.e., small size, medium size, and large size, respectively) were built. Cells were connected to the PMTs with lenses in all cases. The total inner volume, the mass of PSm added to the cell and the measured volume of the sample for each cell are shown in Table 3.

The results obtained in the continuous measurement of distilled water and the  $^3\text{H}$ ,  $^{90}\text{Sr}/^{90}\text{Y}$  and  $^{241}\text{Am}$  standards with the three cells in the Radilevel detector are shown in Table 4. The background count rate increased with the increase in the cell volume as the quantity of PSm increased and, consequently, more cosmic rays were detected. Regarding the detection efficiencies, a significant decrease was observed for  $^3\text{H}$  when the cell size increased, producing values below 0.1% for the large cell. For  $^{90}\text{Sr}/^{90}\text{Y}$  and  $^{241}\text{Am}$ , the differences were not so significant, but a slight decrease was also observed with an increase of the cell size. This decrease in the detection efficiency can be attributed to an increased optical quenching caused by an increase in the distance that photons have to cross through the heterogeneous scintillation medium. Photons produced in the big cell have to cross a high distance to produce signals in both PMT and therefore may be attenuated by the Psm non-diffusive medium. As a consequence, fewer photons arrive at the PMT, thereby decreasing the detection efficiency. This effect was increased for the weak beta emitters, as they produce fewer photons per disintegration than alphas or high energy beta emitters.

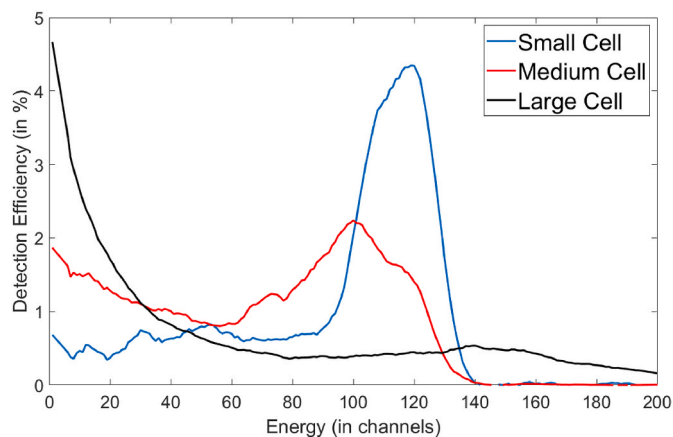


Fig. 5. Detection efficiency for  $^{90}\text{Sr}/^{90}\text{Y}$  using a small, medium and large PS cell.

This hypothesis was confirmed by the  $^{90}\text{Sr}/^{90}\text{Y}$  spectra (Fig. 5). The spectrum obtained using the small cell was located at high energy channels, since the number of photons capable of crossing the entire cell and reaching the PMTs was higher than that in the medium or large cell, which produced spectra located at lower energy channels.

However, when considering the volume of the cell, the cell with a lower width presented the lowest detection efficiency for all the isotopes. In the case of  $^3\text{H}$ , the medium-sized cell presented the best results, whereas for  $^{241}\text{Am}$  and  $^{90}\text{Sr}/^{90}\text{Y}$ , the large cell produced the best results.

According to these results, none of the cells evaluated provided significantly better results than the others, since several factors are relevant in the definition of the limit of detection. It can be said that an optimum cell has to contain the lowest possible amount of PS (or other scintillating material) as the constituent material; photon transmission should be enhanced by means of reflective elements; and the active cell volume must be as high as possible provided that the  $^3\text{H}$  detection efficiency is not reduced too much when the cell is filled.

### 3.2. Shielding evaluation

In the design of the Waterrad detector, two different strategies were considered to reduce the background:

- Passive shielding: an asymmetric box of lead containing a copper box.
- Active shielding: an asymmetric massive block of PS connected to two PMTs.

According to this design, the equipment has four PMTs operating in coincidence, two for the sample detector and two for the active shield detector.

The lead shielding was built using six blocks of an alloy of lead and tin (5%). The block on the top had a height of 10 cm, the block on the bottom had a height of 7.5 cm, and the other four blocks (two on the lateral sides, one at the front and one at the back) had a width of 5 cm. The blocks were coupled and the structure was kept stable by a steel frame, which was placed at the four corners of the lead box. The blocks on the lateral sides had two holes for the PMTs, whereas the block on the front had a square hole through which the detection cell was introduced. The dimensions of the lead box were fixed to contain the PS active shield detector. A door, made of lead and with the same width as that of the hole of the front block, was used to close the detector and ensure optical tightness. The lead door was also coupled to the steel structure and contained two lateral notches for the tubes needed to allow the passage of water through the detection cell.

A copper box (300\*100\*200 mm) was placed inside the lead box to

Table 4

Background count rate (in counts per minute) obtained using different shielding configurations.

Lead shielding and active shielding	63 (2)
Only lead shielding (no active shielding)	151 (1)
Superior lead block and active shielding	1042 (7)
Superior lead block (no active shielding)	1729 (13)
Active shielding (no lead)	1222 (6)
No lead and no active shielding	2062 (3)

attenuate the low-energy X-rays produced from the interaction of the cosmic rays with the lead. Like the lead box, the copper box contained a square hole in the front to allow the entrance of the detection cell and two holes on each side for the PMTs.

A PS block was used as an active shield to remove the cosmic rays that were not suppressed by the lead. The PS blocks were mechanized to contain the two PMTs of the sample detector (which were placed completely inside the PS block) and the detection cell. The entire block was painted with white reflective paint, blank paint and a protective varnish, except the areas where the PMTs of the active shield detector were coupled.

To evaluate the effect of the different elements on reducing the background, measurements were performed using a PS block with the same dimensions as that of the CP cell, with a hole through which a 20-mL polyethylene vial, filled with 16 g of PSM and 8 mL of water, was placed. The results obtained are shown in Table 4. The background was greater when the lead was removed and substituted with POM blocks and the active shielding was deactivated. When the lead blocks were added, the background was reduced by 10 times. This reduction was higher than that achieved with only the activation of the guard detector (only 2 times). Since the background reduction achieved with the lead was higher than that obtained with the active guard and considering the directionality of the cosmic rays, a test was performed to assess passive shielding containing only the top block of lead. In this case, the reduction was only 20% and when the active shielding was activated, the background was reduced to 50% of the initial value. Therefore, despite the directionality of the cosmic rays, all the lead blocks were needed to get an optimum reduction. Finally, when all the lead blocks were used and active shielding was activated, the background was reduced to 63 cpm (97% of the initial value), which was the lowest value.

In conclusion, the use of all elements was necessary to get a maximum reduction of the background. However, the background value obtained was still higher than that obtained in a commercial detector under the same conditions (6.0 cpm). This was due to the PS of the cell and the lenses, which caused a relevant increase in the background. The use of all these strategies to reduce the background did not counteract the effects of the presence of PS. Therefore, the results also the need to avoid the use of PS as a constituent material of the cell, justifying the use of a cell made of a non-scintillating but transparent material.

### 3.3. Detector optimization

From the data obtained in the cell optimization and the evaluation of the shielding strategies, it seemed clear that PS lenses and cells should not be used, but light reflection has to be employed to avoid the reduction in the detection efficiency. Finally, an increase in the cell volume is required to increase the detection efficiency for alpha and high-energy beta emitters when the cell is completely filled. However, this increase should be balanced with the decrease expected for  $^3\text{H}$ .

High-density polyethylene (HDPE) was first considered to build the walls of the cell. HDPE is not a good scintillating material and, therefore, electrons originating from the interaction of the cosmic rays and the walls of the cell will not produce scintillation photons. Moreover, its mechanical properties are appropriate, as its mechanization is not complex and its resistivity to mechanical and chemical damage is high.

**Table 5**

Background values for blank,  $^3\text{H}$ ,  $^{90}\text{Sr}/^{90}\text{Y}$  and  $^{241}\text{Am}$  samples measured with PSm in the Waterrad and commercial detectors.

	Waterrad without the HDPE container	Waterrad with the HDPE container	Quantulus without the HDPE container
Background (cpm)	12.2	12.0	1.1
$^3\text{H}$ Detection efficiency (%)	0.30	0.30	1.12
$^{90}\text{Sr}/^{90}\text{Y}$ Detection efficiency (%)	163	165	181
$^{241}\text{Am}$ Detection efficiency (%)	67	66	77

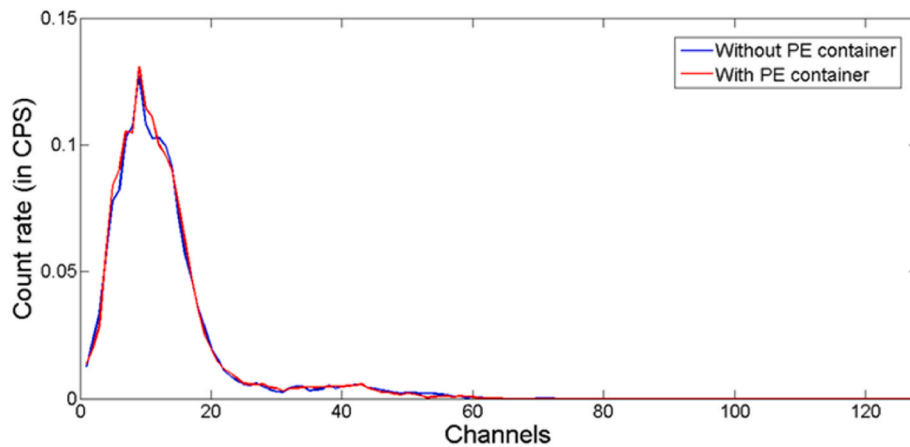


**Fig. 6.** Spectra of a  $^3\text{H}$  sample measured with PSm in the Waterrad detector with or without an HDPE container to hold the vial.

A commercial 7-mL PE vial filled with PSm and different solutions (distilled water,  $^3\text{H}$ ,  $^{90}\text{Sr}/^{90}\text{Y}$  or  $^{241}\text{Am}$ ) was placed in a container made of HDPE and measured in the Waterrad detector. The results obtained were compared to those obtained when the HDPE container was not used and to those obtained in a commercial detector with active and passive shielding (Quantulus) (Table 5).

There were no significant differences in the background nor in the detection efficiencies when comparing the detectors with and without the HDPE container. Moreover, the spectra obtained (Fig. 6) were also in the same position. Therefore, this material can be used to build the cells since it is transparent to scintillation photons and do not produce scintillations through interactions with cosmic rays.

Once the background was reduced, the next improvement was made to the optical transmission. A black POM tube painted with white reflective paint was used to connect the two PMTs of the sample detector. The tube contained a hole at the top and at the bottom to place inside it the cell and the tubing. With this connecting tube, the photons produced in the cell were emitted directly or through reflections on the walls of the connector to the PMTs.

The results obtained with a 20-mL PE vial filled with PSm and different solutions (distilled water,  $^3\text{H}$ ,  $^{90}\text{Sr}/^{90}\text{Y}$  or  $^{241}\text{Am}$ ) in the Waterrad detector were compared to those obtained with using a PS block and PS lenses. As expected, the removal of the PS material produced a significant reduction in the background to levels similar to those

**Table 6**

Background values for blank,  $^3\text{H}$ ,  $^{90}\text{Sr}/^{90}\text{Y}$  and  $^{241}\text{Am}$  samples measured with PSm in the Waterrad detector with a reflective connector or a PS block and PS lenses.

	Waterrad with a reflective connector	Waterrad with a PS block and PS lenses
Background (cpm)	13.3	62.8
$^3\text{H}$ Detection efficiency (%)	0.62	0.51
$^{90}\text{Sr}/^{90}\text{Y}$ Detection efficiency (%)	159	160
$^{241}\text{Am}$ Detection efficiency (%)	61	62

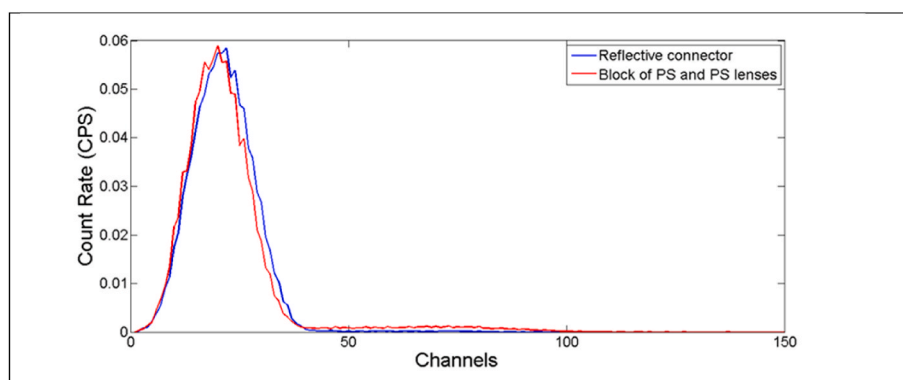


**Fig. 7.** Comparison of the detection efficiencies for  $^3\text{H}$  between a Waterrad detector with a reflective connector and that with a PS block and PS lenses.

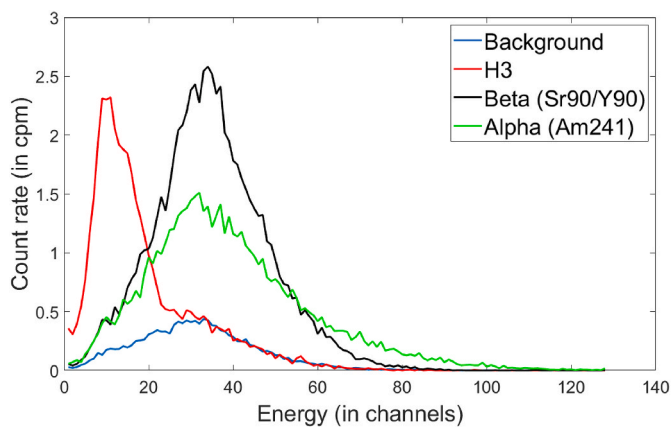


Fig. 8. Spectra for distilled water (background), <sup>3</sup>H, <sup>90</sup>Sr/<sup>90</sup>Y and <sup>241</sup>Am solutions assessed in continuous measurements in the Waterrad detector.

Table 7  
Background (in cps) of the Waterrad detector in the full and optimum windows.

Full spectrum	<sup>3</sup> H window	Beta window	Alpha window
0.23 (1)	0.056 (6)	0.17 (1)	0.23 (1)

of a commercial detector with active and passive shielding (Table 6). Moreover, the detection efficiencies for alpha and high-energy beta emitters were similar, but increased for <sup>3</sup>H, showing that optical transmission was improved.

This was confirmed by the spectra (Fig. 7), which had shifted to high energy channels.

Based on these results, a new cell was built. This chamber was cylindrical to improve the water flow through the whole PSm bed. It was made of HDPE and had an internal diameter of 25 mm (between the medium and large cell sizes) and an internal height of 66 mm. The inner volume of the cell was 32 mL, which corresponded to approximately 21.5 g of PSm and 10.5 mL of the water sample. The cell had four holes on the bottom at which four 0.45-µm filters were located to prevent the entrance of particulate material into the PSm bed. The top of the cell also contained four holes, each one with a 0.45-µm filter, to place the tubes that were connected to the pump. The tubing was coupled to the body of the cell using screws. The cell was placed inside a reflective POM connector and positioned between the two PMTs of the sample.

### 3.4. Waterrad calibration

Calibration of the Waterrad detector was undertaken once the detection cell and the detection chambers were defined and during the optimization of the final set-up of the data handling, hydraulics, remote data sending and operational controls. Three calibration processes were undertaken in this period and each calibration three to seven sequences of measurements. Each sequence was composed of consecutive measurements of distilled water (background), the <sup>3</sup>H standard, the <sup>90</sup>Sr/<sup>90</sup>Y standard (an example of beta-emitting radionuclides) and the <sup>241</sup>Am standard (an example of alpha-emitting radionuclides) in that order. In all the cases, when the cell was filled, the flow was stopped and the measurement started. All these data gave a very precise indication of the stability and robustness of the equipment.

The spectra obtained, with the x axis expressed in energies channels after logarithmic amplification, are shown in Fig. 8. The <sup>3</sup>H spectrum was mainly located in the low energy channels and with a low coincidence with the background spectrum. Background signals were located across the whole spectrum, with a maximum at around channel 30 and with a high coincidence with the <sup>241</sup>Am spectrum. This indicated that the main causes of the background were the high-energy cosmic rays.

Table 8  
<sup>3</sup>H, <sup>90</sup>Sr/<sup>90</sup>Y and <sup>241</sup>Am detection efficiencies of the Waterrad detector.

		<sup>3</sup> H (cps·L·Bq <sup>-1</sup> )	<sup>90</sup> Sr/ <sup>90</sup> Y (cps·L·Bq <sup>-1</sup> )	<sup>241</sup> Am (cps·L·Bq <sup>-1</sup> )
1st sequence (n = 4)	Full window	1.9(4) · 10 <sup>-5</sup>	7.1(2) · 10 <sup>-3</sup>	6.0(4) · 10 <sup>-3</sup>
	Optimum window	1.8(2) · 10 <sup>-5</sup>	6.3(2) · 10 <sup>-3</sup>	6.0(4) · 10 <sup>-3</sup>
2nd sequence (n = 4)	Full window	1.9(2) · 10 <sup>-5</sup>	6.7(2) · 10 <sup>-3</sup>	5.0(4) · 10 <sup>-3</sup>
	Optimum window	1.8(2) · 10 <sup>-5</sup>	5.8(3) · 10 <sup>-3</sup>	5.0(4) · 10 <sup>-3</sup>
3rd sequence (n = 7)	Full window	1.8(1) · 10 <sup>-5</sup>	8.3(5) · 10 <sup>-3</sup>	5.4(5) · 10 <sup>-3</sup>
	Optimum window	1.7(5) · 10 <sup>-5</sup>	7.1(4) · 10 <sup>-3</sup>	5.4(5) · 10 <sup>-3</sup>
Mean	Full window	1.86(7) · 10 <sup>-5</sup>	7.4(8) · 10 <sup>-3</sup>	5.5(5) · 10 <sup>-3</sup>
	Optimum window	1.7(6) · 10 <sup>-5</sup>	6.4(6) · 10 <sup>-3</sup>	5.5(5) · 10 <sup>-3</sup>

Table 9  
Critical level and the detection limit for <sup>3</sup>H, <sup>90</sup>Sr/<sup>90</sup>Y and <sup>241</sup>Am.

		1 h	5 h	24 h
<sup>3</sup> H	Critical level (Bq L <sup>-1</sup> )	540	240	110
	Detection limit (Bq L <sup>-1</sup> )	1123	490	220
Beta ( <sup>90</sup> Sr/ <sup>90</sup> Y)	Critical level (Bq L <sup>-1</sup> )	2.5	1.1	0.5
	Detection limit (Bq L <sup>-1</sup> )	5.1	2.3	1.0
Alpha ( <sup>241</sup> Am)	Critical level (Bq L <sup>-1</sup> )	3.4	1.5	0.7
	Detection limit (Bq L <sup>-1</sup> )	6.9	3.0	1.4

Therefore, the optimum window for <sup>3</sup>H covered only the first channels (2-17), whereas only the central part of the spectrum was considered (19-77) for <sup>90</sup>Sr/<sup>90</sup>Y. For <sup>241</sup>Am, the high coincidence between its spectrum and the background spectrum meant that the entire spectrum was considered (2-127). The optimum window was defined as the area of the spectrum with a higher figure of merit for the specific radionuclide.

The mean background values for the full spectra and the optimum windows obtained in the last calibration process (19 replicate measurements) are shown in Table 7.

The results of the detection efficiencies obtained for the standards from the total spectra and the optimum windows are shown in Table 8.

Considering the mean values obtained for the three sequences and the background in the last sequence, the critical level and detection limit were obtained from the full and optimum windows (Table 9).

For tritium and gross beta, the critical level and detection limit for the different counting times were in the order of magnitude of the parametric values described in the European directive for water intended for human consumption (100 Bq/L for <sup>3</sup>H; 1.0 Bq/L for gross beta

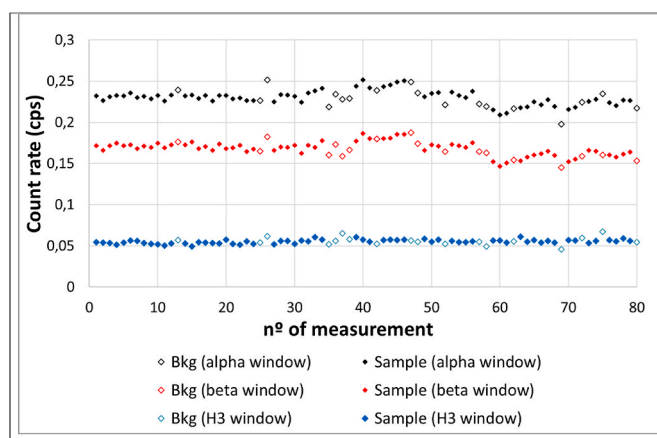


Fig. 9. Count rate profile for background and sample measurements in the optimum windows.

and 0.1 Bq/L for gross alpha). For gross alpha, the values were slightly higher, even at the highest counting time. Nevertheless, these values were still higher than the detection limits established in the European directive. Therefore, the Waterrad detector cannot be used for monitoring of drinking water for the directive purposes, but, as an alarm detector for the daily monitoring of pre-potable water samples with the aim to detect radioactive contaminations with alpha and beta emitting radionuclides at low activity levels, lower than other systems described in the bibliography.

### 3.5. Continuous measurements

A preliminary test of water samples was performed by an automated replicate analysis of water samples from the Ebro River. A 0.45- $\mu\text{m}$  filter was placed after the water reservoir to prevent the entrance of solid material into the cell. The cell was filled with the sample or distilled water and several measurements of 5 min were taken. The sample was measured for 5 h, whereas the background sample was measured only for 1 h. This configuration allowed a fast detection (5') of pulses of activity and the analysis of the sample at activity levels close to the environmental level (5 h).

As can be seen in Fig. 9, the detections presented high stability during the measurement period (15 days) and none of the sample measurements surpassed the critical level.

Full validation of the Waterrad performance (precision and accuracy) would be object of future studies which might include the measurement of several spiked and real samples of different composition and activity.

## 4. Conclusions

A detector for the continuous monitoring of alpha and beta emitters in water samples has been developed. The detector is based on the use of plastic scintillation microspheres to detect radioactivity. Several cells were evaluated and the best results were obtained with a cell made of polyethylene and filled with 20 g of PSm that were 60  $\mu\text{m}$  in diameter. A sample volume of 10 mL was estimated to fill the interstices between the PSm.

Waterrad detector contains and active guard made of PS and a passive shielding made of lead and cooper. Moreover, materials used has been optimized to reduce scintillation signals generated by cosmic radiation. As consequence a low background count rate of 0.23 cps was achieved.

Due to the configuration of the cell and the small size of the scintillator, almost all the cell volume was active. Therefore, the alpha and beta particles emitted from the radionuclides present in a sample could be detected efficiently. The detection efficiencies were 61% and 159% for  $^{241}\text{Am}$  and  $^{90}\text{Sr}/^{90}\text{Y}$ , respectively, indicating that most of the signals were detected. Other factors, such as light transmission, were optimized to enhance the detection efficiency.

The  $^3\text{H}$  radionuclide was very difficult to detect due to its low energy. Most of the systems described to date are not able to detect it or they do with a very low detection efficiency. In the Waterrad detector, the detection efficiency for  $^3\text{H}$  was 0.6%. This value could be improved by using a smaller cell, but this increased the detection limit by decreasing the sample volume.

The Waterrad detector was able to provide a critical level and detection limits in the order of magnitude of the European directive for drinking water for  $^3\text{H}$  and gross beta (220 Bq/L for  $^3\text{H}$ , 0.5 Bq/L for gross beta and 1.4 Bq/L for gross alpha considering 24h measurement). These results demonstrate that the Waterrad detector can be used as an alarm detector for water monitoring to detect low activity radioactive contaminations events. These values are slightly higher to that of the directive (5 times  $^3\text{H}$ , 2.3 times for gross beta and 30 times for gross alpha) but still on the environmental range, making it suitable for water or waste surveillance with low activity alarm purpose involving a high

frequency of measurements (from 1 to 24 measurements per day)."

The detector was tested in an automated analysis with the capacity to perform routine procedures (sample measurement, calibration and cell cleaning). It was able to send the signals remotely, allowing remote sensing.

## CRediT authorship contribution statement

**A. Tarancón:** Writing – review & editing, Writing – original draft, Validation, Methodology, Investigation, Conceptualization. **O. Novella:** Validation, Methodology, Investigation. **M. Pujadas:** Validation, Methodology, Investigation. **M. Batlle:** Validation, Methodology, Investigation. **J. Cros:** Supervision, Project administration, Funding acquisition. **J.F. García:** Writing – review & editing, Supervision, Project administration, Funding acquisition, Conceptualization.

## Declaration of competing interest

The authors declare that they have no known competing financial interests or personal relationships that could have appeared to influence the work reported in this paper.

## Acknowledgments

The authors wish to thank the Spanish Centro para el Desarrollo Industrial, CDTI, del Ministerio de Ciencia e Innovación for financial support under IDI-20100094.

## References

- Azevedo, C.D.R., Baeza, A., Chauveau, E., Corbacho, J.A., Díaz, J., Domange, J., Marquet, C., Martínez-Roig, M., Piquemal, F., Veloso, J.F.C.A., Yahlali, N., 2020. Simulation results of a real-time in water tritium monitor. *Nucl. Instruments Methods Phys. Res. Sect. A Accel. Spectrometers, Detect. Assoc. Equip.* 982, 164555.
- Bliznyuk, V.N., Duval, C.E., Apul, O.G., Seliman, A.F., Husson, S.M., DeVol, T.A., 2015. High porosity scintillating polymer resins for ionizing radiation sensor applications. *Polymer* 56, 271–279.
- Cantaluppi, C., Zannoni, D., Cianchi, A., Giacetti, W., Lovisetto, B., Pagnin, E., Favero, T., 2021. Methods for radioactivity measurements in drinking water using gamma spectrometry. *J. Environ. Radioact.* 232, 106566.
- Currie, I.A., 1968. Limits for qualitative detection and quantitative determination. Application to radiochemistry. *Anal. Chem.* 40 (3), 586–593.
- de España, R., 2016. Real Decreto 314/2016, de 29 de julio, por el que se modifican el Real Decreto 140/2003, de 7 de febrero, por el que se establecen los criterios sanitarios de la calidad del agua de consumo humano, el Real Decreto 1798/2010, de 30 de diciembre, por el que. *Boletín Of. Del Estado*, pp. 60502–60511.
- Hofstetter, K.J., Wilson, H.T., 1992. Aqueous effluent tritium monitor development. *Fusion Technol.* 21, 446–451.
- Hou, X., 2018. *Liquid Scintillation Counting for Determination of Radionuclides in Environmental and Nuclear Application*. Springer International Publishing.
- Hou, X., Roos, P., 2008. Critical comparison of radiometric and mass spectrometric methods for the determination of radionuclides in environmental, biological and nuclear waste samples. *Anal. Chim. Acta* 608, 105–139.
- Hughes, L.D., DeVol, T.A., 2006. Evaluation of flow cell detector configurations combining simultaneous preconcentration and scintillation detection for monitoring of pertechnetate in aqueous media. *Anal. Chem.* 78 (7), 2254–2261.
- Jobbágy, V., Wätjen, U., Merino, J., 2010. Current status of gross alpha/beta activity analysis in water samples: a short overview of methods. *J. Radioanal. Nucl. Chem.* 282, 393–399.
- Köll, Z., 2015. Nuclear Instrument. *Method. Phys. Res. A. Plastic. Scintillator Active. Tritated / $\ell$  range* 798, 24–29.
- L'Annunziata, M.F., 2020. *Handbook of Radioactivity Analysis*, fourth ed. Elsevier, Amsterdam.
- Lee, U., Choi, W.N., Bae, J.W., Kim, H.R., 2019. Fundamental approach to development of plastic scintillator system for in situ groundwater beta monitoring. *Nucl. Eng. Technol.* 51, 1828–1834.
- Lluch, E., Barrera, J., Tarancón, A., Bagán, H., García, J.F., 2016. Analysis of  $^{210}\text{Pb}$  in water samples with plastic scintillation resins. *Anal. Chim. Acta* 940, 38–45.
- Lv, W.H., Yi, H.C., Liu, T.Q., Zeng, Z., Li, J.L., Zhang, H., Ma, H., 2018. Gross beta determination in drinking water using scintillating fiber array detector. *Appl. Radiat. Isot.* 137, 161–166.
- Santiago, L., Bagán, H., Tarancón, A., Rauret, G., García, J.F., 2013. Systematic study of particle quenching in organic scintillators. *Nucl. Instrum. Methods Phys. Res., Sect. A* 698, 26–36.
- Santiago, L.M., Tarancón, A., García, J.F., 2016. Influence of preparation parameters on the synthesis of plastic scintillation microspheres and evaluation of sample preparation. *Adv. Powder Technol.* 27, 1309–1371.

- Sigg, R.A., McCarty, J.E., Livingston, R.R., Sanders, M.A., 1994. Real-time aqueous tritium monitor using liquid scintillation counting. *Nucl. Instrum. Methods Phys. Res., Sect. A* 353 1–3, 494–498.
- Sobiech-Matura, K., Máté, B., Altitzioglou, T., 2017. Radioactivity monitoring in foodstuff and drinking water - an overview of performance of EU laboratories based on interlaboratory comparisons. *Food Control* 72, 225–231.
- Tarancón, A., Kossert, K., 2011. Application of a free parameter model to plastic scintillation samples. *Nucl. Instrum. Methods Phys. Res., Sect. A* 648, 124–131.
- Tarancón, A., García, J.F., Rauret, G., 2007. First approach to radionuclide mixtures quantification by using plastic scintillators. Influence of plastic beads diameter. *Anal. Chim. Acta* 590, 232–238.
- Tarancón, A., Bagán, H., García, J.F., 2017. Plastic scintillators and related analytical procedures for radionuclide analysis. *J. Radioanal. Nucl. Chem.* 555–572.
- Tarancón, A., Padro, A., García, J.F., Rauret, G., 2005. Development of a radiochemical sensor, Part 2: application to liquid effluents. *Anal. Chim. Acta* 538, 241–249.
- the Council of the European Union, 2013. Council Directive 2013/51/Euratom of 22 October 2013 laying down requirements for the protection of the health of the general public with regard to radioactive substances in water intended for human consumption. *Off. J. Eur. Union* 296, 12–21.
- WHO, 2018. Guidelines for Drinking-Water Quality, fourth ed. WHO, Geneva.